Plasma Physics Reports, Vol. 24, No. 7, 1998, pp. 573–583. From Fizika Plazmy, Vol. 24, No. 7, 1998, pp. 621–632.

ELECTRON KINETICS AND APPLICATIONS OF GLOW DISCHARGES

Comprehensive Three-Dimensional Modeling Network for a DC Glow Discharge Plasma[1]

A. Bogaerts and R. Gijbels

Department of Chemistry, University of Antwerp, Universiteitsplein 1, B-2610 Wilrijk-Antwerp, Belgium

Received August 21, 1997

Abstract—A set of three-dimensional models for different species present in a glow discharge plasma has been developed. The models are all coupled to each other by the interaction processes between the various species, and the resulting comprehensive modeling network is solved iteratively until final convergence is reached. An overview table summarizing the typical results of the models is presented, some of which are illustrated in more detail.

1. INTRODUCTION

Glow discharges are used in a large number of application fields, ranging from the microelectronics industry (for deposition of thin films and for plasma etching and modification of surfaces) to the lighting industry and metal-vapor ion laser and plasma display technology. Moreover, they also find applications in analytical chemistry as spectroscopic sources for mass spectrometry and optical emission spectroscopy. To improve results in all these fields, a clear insight into the fundamental processes taking place in the glow discharge is desirable. This can be obtained by modeling the glow discharge processes. We have developed a comprehensive modeling network, consisting of different models for the various species present in glow discharge plasma. In Section 2, a short overview of these models will be given. The coupling of the various models will be presented in Section 3. Section 4 deals with some typical results. Finally, a conclusion is given in Section 5.

2. OVERVIEW OF THE MODELS

The models are, first of all, intended to describe glow discharge plasmas used in analytical chemistry. In this application, the cathode of the glow discharge is constructed out of the material to be analyzed. Ions and fast atoms from the plasma can sputter away cathode material when bombarding the cathode. These sputtered atoms arrive in the plasma, where they can be ionized and/or excited. Therefore, the glow discharge plasma can be considered as an atom and ion reservoir with a composition characteristic for the material to be analyzed (i.e., the cathode). The ions can be measured with a mass spectrometer, whereas the characteristic photons produced by the excitation and subsequent radiative deexcitation processes can be detected by optical emission spectrometry.

[1] This article was submitted by the authors in English.

The species assumed to be present in the plasma include argon atoms at rest, uniformly distributed throughout the discharge; electrons (subdivided into two different groups: fast electrons with energies large enough to produce inelastic collisions and slow electrons), singly charged argon ions; fast argon atoms created from the argon ions by symmetric charge transfer and elastic collisions; argon atoms at various excited levels (65 in total), with special emphasis on the metastable levels; and atoms and ions of the cathode material (i.e., the material to be analyzed).

These species are described by a combination of Monte Carlo and fluid models. Species that are more or less in equilibrium with the electric field are described with a fluid approach, whereas species that are far from equilibrium with the electric field in the discharge are studied with a Monte Carlo simulation.

The fast electrons are treated with a Monte Carlo model [1–3]; collision processes incorporated are elastic collisions with argon atoms, electron–electron Coulomb collisions, electron impact excitation, deexcitation and ionization from the argon ground state and from the various excited levels, as well as ionization of sputtered cathode atoms. The behavior of the thermalized electrons and the argon ions is calculated in a fluid model [2, 3]; the continuity and transport (based on diffusion and migration) equations are coupled with the Poisson equation to obtain a self-consistent electric field distribution throughout the discharge. The electrons are actually split up into two electron groups, based on energy considerations. The behavior of the fast electrons (which are able to produce inelastic collisions) is described explicitly by a Monte Carlo method, as explained above, whereas the thermal electrons are handled in a fluid model. For the latter group, the Maxwellian energy distribution is assumed when solving the fluid model. Hence the equations for the thermal electrons considered in this fluid model, are conservation of number density and transport by diffusion and

1063-780X/98/2407-0573$15.00 © 1998 МАИК Наука/Interperiodica Publishing

migration; no separate equation for conservation of energy is included. However, when describing the behavior of the various excited levels of argon, calculation of the detailed ionization, excitation and deexcitation processes of the various levels are required; for that purpose, the Monte Carlo model is used not only for the fast electron group, but for all electrons. For example, Fig. 4 will present the electron energy distribution calculated with the Monte Carlo model for all electrons (see below). The argon ions are described with a Monte Carlo model in the cathode dark space (CDS), as well as the fast argon atoms, which are created by symmetric charge transfer and elastic collisions from the argon ions, because these species are not in equilibrium with the electric field in this region [1, 4]. The collision processes taken into account are symmetric charge transfer for the argon ions, elastic collisions with argon atoms for both argon ions and fast atoms (strictly speaking, symmetric charge transfer is also a form of elastic collision, because there is no change in internal energy of the colliding species [5]), and fast argon ion and atom impact ionization, and excitation and deexcitation of argon atoms in the ground state and in the different excited levels. The argon metastable atoms are handled with a fluid model consisting of different production and loss processes [6, 7]. The production processes incorporated are electron, argon ion, and atom impact excitation to the metastable levels and electron–ion radiative recombination. The loss processes include electron impact excitation and ionization from the metastable levels, electron collisional transfer to the nearby resonant levels, Penning ionization of the sputtered cathode atoms, metastable atom–metastable atom collisions, and two-body and three-body collisions with argon ground state atoms. An additional loss process is diffusion and subsequent deexcitation at the cell walls. The behavior of the various argon excited levels is calculated in a kind of fluid model, i.e., a so-called collisional–radiative model, because the level populations of the different excited states are determined by a range of collisional and radiative processes [8]. The relevant processes taken into account are radiative decay; electron, fast argon ion, and fast and thermal argon atom impact ionization; excitation and deexcitation between all the levels; electron–ion radiative recombination; and electron–ion three-body recombination where the third body is an electron, fast argon ion, or a fast or thermal argon atom. Resonance radiation transport is accounted for in the model by the incorporation of radiation trapping; i.e., the photons emitted due to radiative decay of excited levels to the ground state can be reabsorbed again by the ground state atoms, so that only a small fraction can escape and the majority is trapped. The so-called "escape factor" is calculated according to the method of Holstein [9] and Walsh [10] and is on the order of 10^{-3} to 10^{-4} for the typical pressures investigated. The sputtered cathode atoms (copper is chosen here as an example) leave the cathode with energies of 5–10 eV; they lose these energies almost immediately by collisions with argon atoms, until they are thermalized. This thermalization process is described with a Monte Carlo model [11]. The further transport of the cathode atoms (diffusion-controlled), their ionization, and the transport of the cathode ions (determined by diffusion and migration in the electric field) is described with a fluid model [7, 12]; the ionization processes considered for the sputtered atoms are Penning ionization by argon metastable atoms, asymmetric charge transfer by argon ions, and electron impact ionization. Finally, since the cathode ions are not in equilibrium with the electric field in the CDS, they are also treated in this region with a Monte Carlo model [7, 12].

The Monte Carlo models are developed in three dimensions, whereas the fluid models could be handled in two dimensions. Indeed, due to the cylindrical symmetry of the cells to which the models are applied, the three dimensions could be reduced to two dimensions. More information about the models can be found in [1–8, 11–13].

3. COUPLING OF THE MODELS

The different models are coupled to each other by the interaction processes between the different plasma species. The models are therefore combined into a comprehensive modeling network and solved together by an iterative procedure in order to obtain an overall picture of the glow discharge. The flow chart of the coupling is presented in Fig. 1.

The procedure starts with the argon ion–slow electron fluid model, assuming arbitrary creation rates of argon ions and slow electrons (R_{Ar^+} and $R_{e,\,slow}$). Results of this model are, among others, (i) the axial and radial electric field distributions throughout the discharge (E_{ax} and E_{rad}); (ii) the interface between cathode dark space (CDS) and negative glow (NG) for all radial positions ($d_c(r)$, defined as the position where the calculated potential goes through zero); (iii) the argon ion flux entering the CDS ($j_{Ar^+,\,d_c}(r)$); and (iv) the argon ion flux bombarding the cathode ($j_{Ar^+,\,0}(r)$), both as a function of the radial position.

This information is used in the Monte Carlo models. From the argon ion flux bombarding the cathode, the electron flux starting at the cathode as a function of the radial position is obtained: $j_{e,\,0}(r) = -\gamma j_{Ar^+,\,0}(r)$, where γ is the ion-induced secondary electron emission coefficient. The fast electron Monte Carlo model is calculated and yields, among others, the ionization rate of argon atoms (i.e., the creation rate of argon ions) by electron impact as a function of axial and radial positions ($R_{e,\,ion,\,Ar}$).

This is used in the argon ion and fast atom Monte Carlo model as the number of argon ions created in the CDS. The argon ion flux starting at the interface

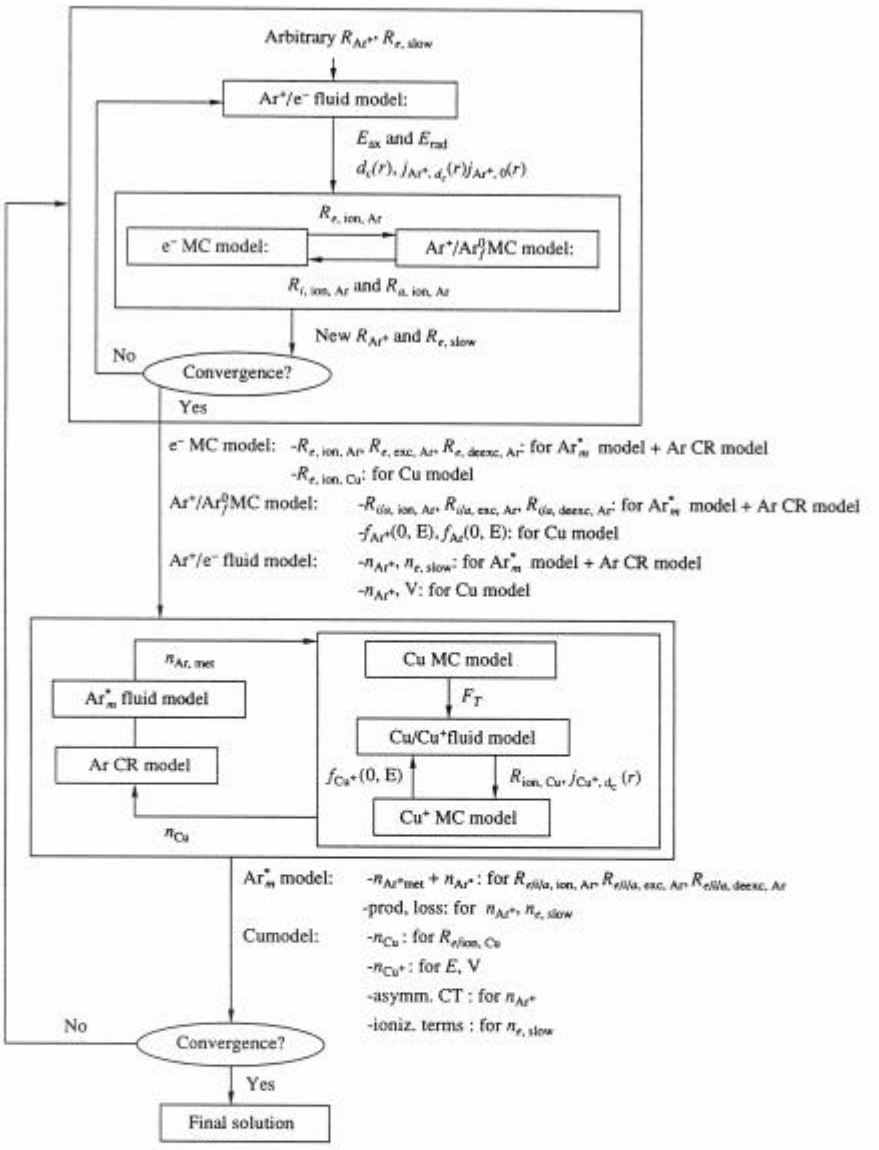

Fig. 1. Flowchart of the combined models.

between CDS and NG as a function of radial position, is obtained from the argon ion–slow electron fluid model ($j_{Ar^+,\,d_c}(r)$, see above). Outputs of the argon ion and fast atom Monte Carlo model are, among others, the argon ion and atom impact ionization rates (i.e., the creation rates of electrons, $R_{i,\,ion,\,Ar}$ and $R_{a,\,ion,\,Ar}$).

Next, the fast electron Monte Carlo model is calculated again, incorporating these electrons formed by argon ion and atom impact ionization. With the new creation rate of argon ions (i.e., by electron impact ionization), the argon ion and fast atom Monte Carlo model is again calculated. This is repeated until convergence is reached (i.e., when the argon ion flux bombarding the cathode, calculated in the argon ion and fast atom Monte Carlo model, does not change anymore). This is generally achieved after two or three iterations.

The creation rate of the slow electrons ($R_{e,\,slow}$), resulting from the electron Monte Carlo model and the argon ion creation rates ($R_{Ar^+} = R_{e,\,ion,\,Ar} + R_{i,\,ion,\,Ar} + R_{a,\,ion,\,Ar}$), calculated in the electron and argon ion and

fast atom Monte Carlo models are used as inputs in the argon ion–slow electron fluid model. This yields new axial and radial electric field distributions, a new interface between CDS and NG, and new argon ion fluxes entering the CDS and bombarding the cathode. This information is again put into the Monte Carlo models. The whole procedure is repeated until final convergence is reached (i.e., generally after five to ten iterations).

Results of the electron, argon ion, and fast atom Monte Carlo models and of the argon ion–slow electron fluid model, which are of importance for the argon metastable atom fluid model (Ar_m^* model); the excited-level argon collisional–radiative model (Ar CR model); and for the three copper models are the following.

The electron Monte Carlo model yields the electron impact ionization, excitation, and deexcitation rates between all the excited levels ($R_{e,\,\mathrm{ion,\,Ar}}$, $R_{e,\,\mathrm{exc,\,Ar}}$, $R_{e,\,\mathrm{deexc,\,Ar}}$), which are used as populating and depopulating terms in the argon metastable atom fluid model and the argon collisional–radiative model. It also gives the electron impact ionization rate of copper atoms ($R_{e,\,\mathrm{ion,\,Cu}}$), which is used as loss term for the copper atoms and production term for the copper ions in the copper atom and ion fluid model.

The argon ion and fast atom Monte Carlo model calculates the argon ion and atom impact ionization, excitation, and deexcitation rates between all the argon atom levels ($R_{i/a,\,\mathrm{ion,\,Ar}}$, $R_{i/a,\,\mathrm{exc,\,Ar}}$, $R_{i/a,\,\mathrm{deexc,\,Ar}}$), which are populating and depopulating terms in the argon metastable atom fluid model and the argon collisional–radiative model. They also give the argon ion and atom flux energy distributions at the cathode ($f_{\mathrm{Ar}^+}(0, E)$ and $f_{\mathrm{Ar}}(0, E)$), which are needed to calculate the flux of sputtered copper atoms in the copper ion and atom fluid model.

Finally, the argon ion–slow electron fluid model yields the argon ion and slow electron densities (n_{Ar^+} and $n_{e,\,\mathrm{slow}}$), which are exploited in some populating and depopulating terms of the argon metastable atom fluid model and the argon collisional–radiative model (i.e., electron–argon ion recombination to all levels). Moreover, the argon ion density and the potential distribution (V) resulting from the argon ion–slow electron fluid model are made use of in the copper atom and ion fluid model for the asymmetric charge transfer ionization and for the migration component of the copper ion transport, respectively.

With these input values, the argon metastable atom fluid model, the argon excited-level collisional–radiative model, and the copper models are solved. The argon metastable atom model and the collisional–radiative model for the other excited levels are coupled, because the population densities of the different excited levels are connected by the various collisional and radiative processes. Furthermore, the argon metastable atom model yields the argon metastable atom density ($n_{\mathrm{Ar,\,met}}$), which is required for the Penning ionization rate of the copper atoms in the copper atom and ion fluid model. Then, the copper models are calculated. The Monte Carlo model of the copper atom thermalization process yields the thermalization profile (F_T), which is the input in the copper atom and ion fluid model. Results of the copper atom and ion fluid model are, among others, the flux of copper atoms entering the CDS ($j_{\mathrm{Cu}^*,\,d_c}(r)$) and the number of copper ions created in the CDS ($R_{\mathrm{ion,\,Cu}}$), which are both needed in the copper ion Monte Carlo model. One of the results of the copper ion Monte Carlo model is the flux energy distribution of the copper ions bombarding the cathode ($f_{\mathrm{Cu}^+}(0, E)$). This allows us to calculate the updated flux of copper atoms sputtered from the cathode used in the copper atom and ion fluid model. The copper atom Monte Carlo model, copper atom and ion fluid model, and copper ion Monte Carlo model are solved iteratively until convergence is reached (typically after two to three iterations). Then, the resulting copper atom density (n_{Cu}) is put into the argon metastable atom fluid model for the Penning ionization loss term. The argon metastable atom fluid model, the argon collisional–radiative model, and the three copper models are solved iteratively until convergence, which is typically reached after two iterations.

Results of the argon metastable atom fluid model, the argon collisional–radiative model, and the three copper models, which can in principle influence the results in the electron, argon ion, and fast atom Monte Carlo models and in the argon ion–slow electron fluid model, are the following.

The argon metastable atom fluid model and the argon collisional–radiative model yield the argon metastable atom density and the population densities of the other excited levels, which are used to recalculate the electron, fast argon ion, and atom impact excitation, deexcitation, and ionization rates in the electron, fast argon ion, and atom Monte Carlo models. Moreover, some of the production and loss terms can influence the argon ion and slow electron densities in the argon ion–slow electron fluid model, although this effect is almost negligible.

The copper atom and ion fluid model yields the copper atom density, which determines the new electron impact ionization rate of copper atoms in the electron Monte Carlo model. The copper ion density can influence the electric field and potential distributions in the argon ion–slow electron fluid model. The asymmetric charge transfer ionization term can affect the argon ion density in the argon ion–slow electron fluid model, and the three ionization terms of copper can influence the slow electron density in the argon ion–slow electron fluid model.

These data are again put into the electron, argon ion, and fast atom Monte Carlo models and into the argon

ion–slow electron fluid model, and the entire model is solved until final convergence is reached. The effects of the argon metastable atom fluid model, the argon collisional–radiative model, and the copper models are, however, negligible at the discharge conditions investigated in this work, so that final convergence is actually already reached after one iteration.

The program source codes are written in Fortran. The calculations are performed on a Sun Sparcserver 20 workstation. The Monte Carlo models typically take about 10 min each in simulating about 10 000 particles. The solution of the coupled equations in the argon ion–slow electron fluid model requires at least 3 h. The calculations in the argon metastable atom fluid model and in the copper atom–copper ion fluid model each take about 1 min, and the collisional–radiative model for the 65 effective levels of the argon atom requires about 1 h.

The whole iteration procedure until final convergence therefore continues several days.

4. RESULTS OF THE MODELS

Table 1 presents an overview of the typical results that have been obtained with the models, as well as the references of papers where more detailed information can be found. In the following, only some results will be selected and illustrated as typical examples of the possibilities of the models.

Figure 2 presents the two-dimensional copper atom density distribution throughout the discharge of the standard cell for analyzing flat samples in the VG9000 glow discharge mass spectrometer (VG Elemental, Thermo Group). The cathode is situated at $z = 0$, and the anode is given by the cell walls (i.e., other boundaries of the figure). Moreover, the black rectangles from $z = 0.05$ to $z = 0.15$ cm represent the so-called front plate of the cell, which is also at anode potential. Cathode and anode are separated by an insulating teflon ring, which is visualized by the black rectangles from $z = 0$ to $z = 0.05$ cm in the figure. It can be seen that the sputtered copper atom density reaches a maximum at about 1 mm from the cathode and decreases gradually towards the cell walls. Three-dimensional sputtered atom density profiles have recently been measured for tantalum atoms with both laser-induced fluorescence and atomic absorption spectrometry, and the experimental results were in excellent agreement with the calculation results at the same discharge conditions and in the same geometry [18].

With the models, it is also possible to calculate the self-consistent potential and electric field distributions throughout the discharge resulting from Poisson's equation, as was illustrated e.g., in [3]. The position at which the potential crosses zero is defined as the interface of cathode dark space (CDS) and negative glow (NG). In Fig. 3, the length of the CDS is illustrated as a function of pressure and voltage for typical discharge conditions encountered in analytical glow discharges.

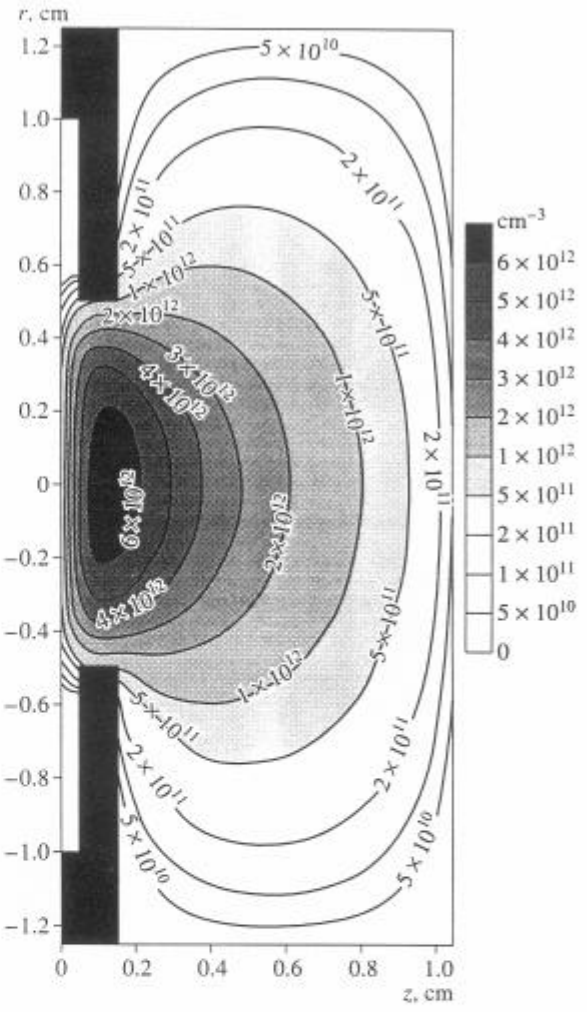

Fig. 2. Calculated two-dimensional density profile of the sputtered copper atoms (glow discharge conditions: p = 0.56 torr, V = 1000 V, I = 3 mA).

The CDS length clearly increases with decreasing pressure and only slightly with decreasing voltage. At lower pressures and voltages, the CDS would fill up the entire discharge region. These calculated results were compared with an empirical relation between the CDS length and the current density in the discharge proposed by Aston [19], and good agreement was reached [4, 13].

With the Monte Carlo models, information can also be obtained about the energy distributions of the plasma species. Figure 4 shows the calculated electron energy distribution as a function of distance from the cathode at $p = 1$ torr, $V = 1000$ V, and $I = 2$ mA. For the present purpose, all electrons with energies ranging from zero to maximum energy (i.e., 1000 eV), and not

Table 1. Overview of the information that can be obtained with the models

Calculated quantities (+ references for more information)	
Electrical current (as a function of voltage and pressure)	(4, 13)
3D potential distributions	(2, 3, 13)
3D axial and radial electric field distributions	(2, 3, 13)
Value of the plasma potential	(2, 3, 13)
Lengths of the different regions (CDS, NG, AZ)	(2, 3, 13)
3D density profiles of	
argon ions	(2, 3, 13)
fast argon atoms	(1, 13)
argon metastable atoms	(6, 7, 8, 13)
other argon excited levels	(8)
fast electrons	(1, 2, 3, 13)
thermalized electrons	(2, 3, 13)
atoms of the cathode material	(7, 12, 13)
ions of the cathode material	(7, 12, 13)
(Thermalized argon atoms are assumed to be uniformly distributed throughout the discharge)	
Ion fluxes of argon and cathode ions at the exit slit of the cell to the mass spectrometer	(14, 15)
Ionization degrees of argon and cathode atoms	(12, 13)
3D energy distributions and mean energies of	
electrons	(1, 2, 13)
argon ions	(1, 13)
fast argon ions	(1, 13)
cathode ions	(12, 13)
Information about collision processes	
3D collision rates of the different collision processes of electrons, argon ions, and fast argon atoms and relative importance of these collision processes	(1–4, 13)
3D rates of Penning ionization, asymmetric charge transfer, and electron impact ionization and relative contributions to the total ionization of sputtered atoms	(7, 12, 13)
3D rates and relative contributions of the various populating and depopulating processes (see text) of the metastable and other excited argon levels	(6, 7, 8, 13)
Information about sputtering	
Sputtering (erosion) rates at the cathode	(7, 12, 13, 16)
Thermalization profiles of the sputtered atoms	(11, 13)
Amount of redeposition on the cathode by backscattering or backdiffusion	(11, 13, 16)
Relative contributions of argon ions, fast argon atoms, and cathode ions to the sputtering process	(1, 7, 12, 13)
2D crater profiles due to sputtering at the cathode	(16)
Emission spectra and emission profiles due to radiative decay from the excited levels	(8)
Prediction of variations in relative sensitivity factors for GDMS	(17)

only the fast electron group (see Section 2), are treated with the Monte Carlo model. At the cathode ($z = 0$), the electrons have rather low energies (around 4 eV) but their energy increases when they move away from the cathode due to the strong electric field in the CDS. However, they also lose energy by collisions and are therefore characterized by a complete distribution ranging from thermal to maximum energy, with all energies of nearly equal probability. Further, in the NG (i.e., starting from 0.15 cm in the present case), the electrons do not gain much energy anymore due to the very weak electric field but they lose their energy more efficiently

by collisions. Hence, the energy distribution shifts towards lower energies and a pronounced peak appears at about 0.4–2 eV. Indeed, when the electrons reach energies of a few eV, they have a large probability for electron-electron Coulomb scattering and they exchange their energy very efficiently with other electrons, leading to a nearly Maxwellian distribution at low energies. However, there are still electrons present with energies ranging up to 1000 eV. The energy distribution is similar in the entire NG region, because the electrons scatter back and forth.

Figure 5 illustrates the argon ion energy distribution, for different positions from the cathode, calculated at the same discharge conditions of Fig. 4. The ions enter the CDS from the NG (at 0.15 cm) with thermal energy (not presented here), but they gain energy on their way towards the cathode. However, they also lose their energy very efficiently due to collisions, so that their energy distribution decreases more or less exponentially towards higher energies. Flux energy distributions of the argon ions bombarding the cathode have also been measured with a double focusing mass spectrometer by varying the acceleration voltage and keeping the magnetic field constant [20], and the results were in rather good agreement with the present calculation results.

The "fast" argon atom energy distribution for different positions from the cathode and at the same discharge conditions as Figs. 4 and 5 is depicted in Fig. 6. It is comparable to the argon ion energy distribution, because the atoms are formed out of the ions by symmetric charge transfer and elastic collisions. However, the energy distribution decreases even more rapidly towards higher energies, since the atoms cannot gain energy from the electric field; they can only lose their energy by collisions. Hence, most fast argon atoms have really low (nearly thermalized) energies.

From the calculated flux energy distributions of the species bombarding the cathode, the amount of sputtering at the cathode can be calculated. From Figs. 5 and 6, it appears that the flux of fast argon atoms is definitely higher than the flux of argon ions. Therefore, it is expected that the fast argon atoms play a dominant role in sputtering. This is indeed observed in Fig. 7, where the relative contributions to sputtering of the fast argon atoms, argon ions, and copper cathode ions as a function of voltage and pressure are illustrated. The fast argon atoms are dominant at all voltages and pressures (i.e., about 70%). The argon ions always take the second place (i.e., about 25–30%). However, the contribution of copper ions to the sputtering (i.e., called "self-sputtering") cannot be neglected. It amounts to about 0.1–5% and clearly increases with voltage and pressure. Indeed, it was found that, at higher voltages and pressures, the ratio of copper ion to argon ion density and flux increases [13] and hence the amount of self-sputtering will rise too.

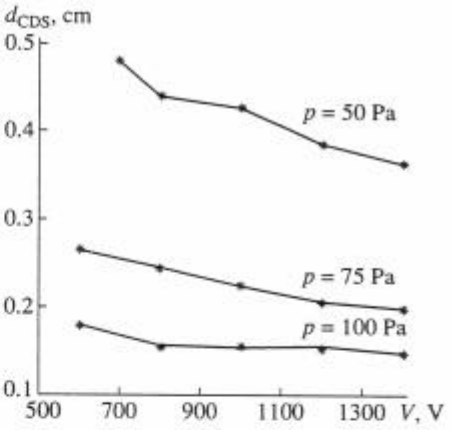

Fig. 3. Calculated length of the cathode dark space (d_{CDS}) as a function of voltage at three pressures.

Finally, Table 2 lists some information about the collision processes of electrons, argon ions and, atoms, which is also obtained from the Monte Carlo models. It was calculated that the electrons undergo about 10–24 collisions per cm in the CDS and about 35–900 per cm in the NG. This high number in the NG is almost entirely due to the very efficient electron–electron Coulomb scattering; this process is nearly absent in the CDS, because the electrons gain energy by the electric field and they have too high energies for efficient electron–electron scattering. Hence, the number of electron–electron collisions is virtually zero in the CDS and ranges from 20 to 900 per cm in the NG. The number of elastic collisions with argon atoms per cm is about 5–20 in both CDS and NG. Electron impact ionization from the ground state level occurs about one to four times per cm in the CDS and less than once per cm in the NG due to the lower energies in this region (and hence less favorable for ionization). The other processes are still less frequent. Integrated over the total discharge region, electron–electron collisions are by far the dominant collision processes (ca. 99%, as appears from Table 2); they are, however, only significant at low (< a few eV) energies. At higher energies, the elastic collisions with argon atoms are the most important processes; but integrated over all energies, they contribute only about 0.73%. The other collision processes (ionization, excitation, deexcitation from the different levels, and recombination to the levels) are of still lower numerical importance, as can be seen from Table 2.

The argon ions undergo about 100–150 collisions per cm, which means about 15–20 collisions in the CDS (since the latter was about 0.15 cm long in the present case). The dominant processes are symmetric charge transfer (ca. 52%) and elastic collisions with argon atoms (ca. 46%). Ionization and total excitation from the ground state level contribute about 0.2 and

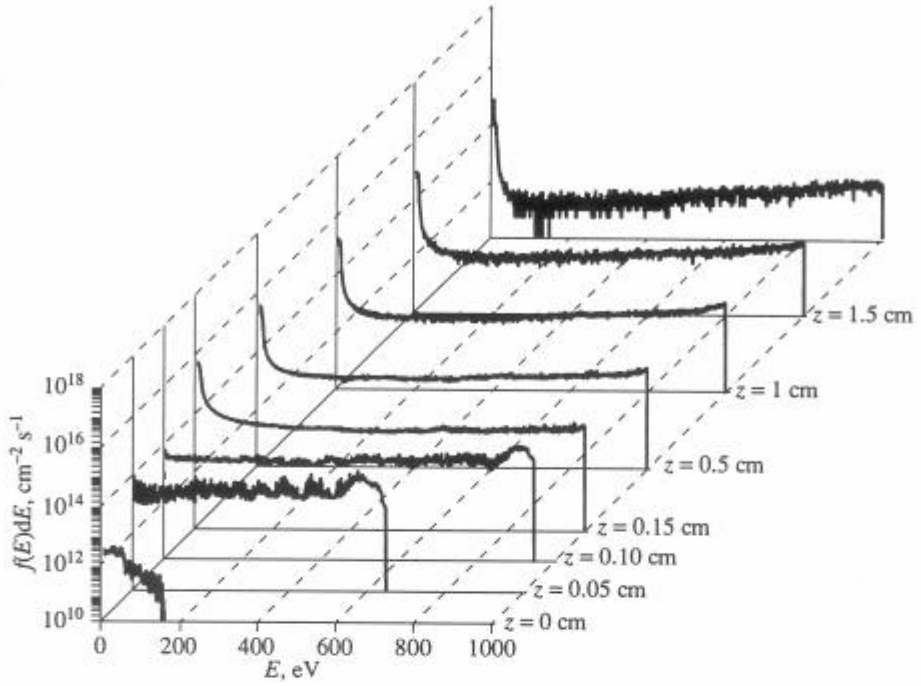

Fig. 4. Calculated flux energy distributions of the electrons as a function of distance from the cathode (glow discharge conditions: p = 1 torr, V = 1000 V, I = 2 mA).

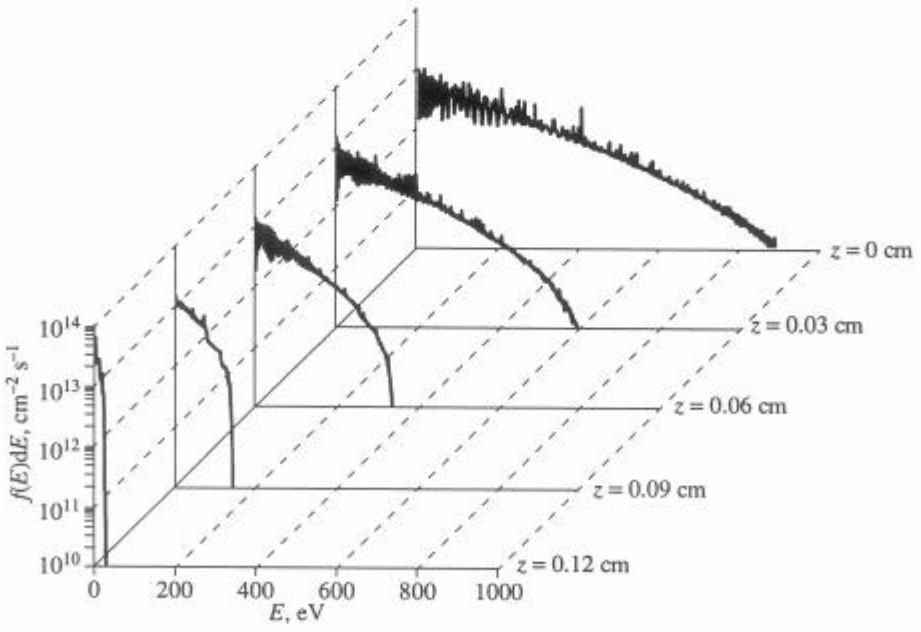

Fig. 5. Calculated flux energy distributions of the argon ions in the CDS as a function of distance from the cathode (glow discharge conditions: p = 1 torr, V = 1000 V, I = 2 mA).

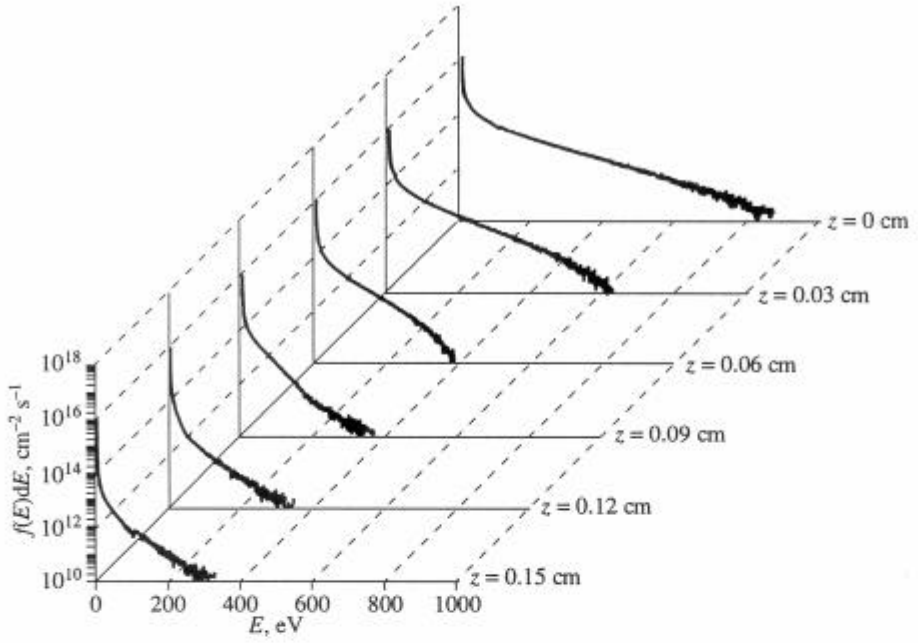

Fig. 6. Calculated flux energy distributions of the fast argon atoms in the CDS as a function of distance from the cathode (glow discharge conditions: $p = 1$ torr, $V = 1000$ V, $I = 2$ mA).

1.2%, respectively; and ionization, excitation and deexcitation from higher levels, and recombination can be considered negligible. The situation is similar for the fast argon atoms: they undergo about 40–60 collisions per cm (hence about 6–9 collisions in the total CDS). These are mainly elastic collisions with argon atoms (ca. 99.4%); ionization and excitation from the ground state level have a minor contribution (i.e., 0.1 and 0.48%, respectively), and the other processes are again of minor numerical importance.

The extent to which both the argon ions and fast atoms give rise to ionization and excitation processes is only of minor importance compared to symmetric charge transfer and elastic collisions. Compared to electron impact ionization and excitation, these processes are, however, not negligible. Indeed, we found that the maximums in the ionization rates by argon ion and atom impact ionization are of the same order of magnitude as the maximum in the electron impact ionization rate at the typical discharge conditions of 0.5–1 torr, 1000 V, and a few milliamps [13]. Integrated over the total discharge region, the relative importances of these processes to the total ionization of argon were calculated to be about 89% for electron impact (about 15% in the CDS and about 74% in the NG), about 2.5% for argon ion impact, and about 8.5% for fast argon atom impact. Hence, in spite of the fact that electron impact ionization is clearly dominant (since it can occur in the entire discharge region, whereas argon ion and atom impact ionization only take place close to the cathode, where the ions and atoms can reach high enough energies), argon ion and atom impact ionization are not negligible at the discharge conditions investigated.

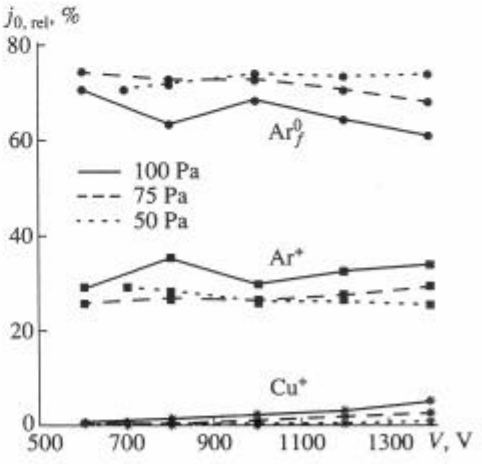

Fig. 7. Calculated contributions to sputtering of the cathode by fast argon atoms, argon ions, and copper cathode ions as a function of voltage at three pressures.

Table 2. Number of collisions per cm for the electrons, argon ions, and fast argon atoms and relative contributions of the different collisions processes incorporated in the model (for a glow discharge cell of 2 cm length and 4 cm radius, at 1 torr pressure, 1000 V discharge voltage, and 2 mA current)

	Electrons	Argon ions	Argon atoms
Total number of collisions, per particle per cm	10–24 in CDS 35–900 in NG	100–150 in CDS	40–60 in CDS
Relative contribution of individual collisions (%):			
electrons: electron–electron scattering	99.0		
ions: symmetric charge transfer		52.3	
elastic collisions	0.73	46.2	99.4
ionization from $n = 1$ (ground state)	0.03	0.2	0.08
excitation from $n = 1$ to 4s ($n = 2$–5)	0.003	1	0.4
excitation from $n = 1$ to 4p ($n = 6$–11)	0.001	0.2	0.07
excitation from $n = 1$ to 3d, 5s ($n = 12$–17)	0.001	0.015	0.004
excitation from $n = 1$ to 5p ($n = 18, 19$)	6×10^{-4}	0.003	8×10^{-4}
excitation from $n = 1$ to 4d, 6s ($n = 20, 21$)	6×10^{-4}	0.005	0.001
excitation from $n = 1$ to higher levels	5×10^{-4}	0	0
ionization from 4s ($n = 2$–5)	10^{-5}	2×10^{-5}	7×10^{-6}
ionization from 4p ($n = 6$–11)	10^{-8}	4×10^{-8}	2×10^{-8}
ionization from 3d, 5s ($n = 12$–17)	3×10^{-8}	10^{-7}	5×10^{-8}
ionization from 5p ($n = 18, 19$)	5×10^{-8}	3×10^{-7}	1.5×10^{-7}
ionization from 4d, 6s ($n = 20, 21$)	8×10^{-8}	8×10^{-7}	4×10^{-7}
ionization from higher levels	2×10^{-5}	10^{-5}	5×10^{-6}
(de)excitation within excited levels	10^{-16}–5×10^{-4}	10^{-20}–10^{-3}	10^{-21}–10^{-3}
recombination to different levels	10^{-16}–10^{-8}	10^{-20}–10^{-11}	10^{-20}–10^{-9}

Besides the three above ionization mechanisms, two other processes incorporated in the model can, in principle, be responsible for the formation of argon ions, i.e., electron impact ionization from the metastable levels and metastable atom–metastable atom collisions leading to the ionization of one of the atoms. However, at the discharge conditions of interest to us, both these processes are found to be only of minor importance (i.e., contribution of 1% or less).

5. CONCLUSION

A comprehensive modeling network consisting of different submodels for the various species present in a glow discharge plasma, has been developed for a DC glow discharge in argon. This paper presents an overview of the different models and explains how the models are coupled to each other and solved iteratively, in order to obtain an overall picture of the glow discharge. The typical results that can be achieved with the models are summarized, and some of them are illustrated in more detail. In general, good agreement is reached between our calculated results and experimental observations, which shows that our models present a more or less realistic picture of the glow discharge plasma.

ACKNOWLEDGMENTS

A. Bogaerts is grateful to the Flemish Fund for Scientific Research (FWO) for financial support. This research is also sponsored by the Federal Services for Scientific, Technical and Cultural Affairs (DWTC/SSTC) of the Prime Minister's Office through IUAP-IV (Conv. P4/10).

REFERENCES

1. Bogaerts, A., van Straaten, M., and Gijbels, R., *Spectrochim. Acta, Part A*, 1995, vol. 50, p. 179.
2. Bogaerts, A., Gijbels, R., and Goedheer, W.J., *J. Appl. Phys.*, 1995, vol. 78, p. 2233.
3. Bogaerts, A., Gijbels, R., and Goedheer, W.J., *Anal. Chem.*, 1996, vol. 68, p. 2296.
4. Bogaerts, A. and Gijbels, R., *J. Appl. Phys.*, 1995, vol. 78, p. 6427.
5. Phelps, A.V., *J. Appl. Phys.*, 1994, vol. 76, p. 747.
6. Bogaerts, A. and Gijbels, R., *Phys. Rev. A*, 1995, vol. 52, p. 3743.

7. Bogaerts, A. and Gijbels, R., *Anal. Chem.*, 1996, vol. 68, p. 2676.
8. Bogaerts, A., Gijbels, R., and Vlcek, J., *J. Appl. Phys.*, 1998, vol. 84 (in press).
9. Holstein, T., *Phys. Rev.*, 1951, vol. 83, p. 1159.
10. Walsh, P.J., *Phys. Rev.*, 1959, vol. 116, p. 511.
11. Bogaerts, A., van Straaten, M., and Gijbels, R., *J. Appl. Phys.*, 1995, vol. 77, p. 1868.
12. Bogaerts, A. and Gijbels, R., *J. Appl. Phys.*, 1996, vol. 79, p. 1279.
13. Bogaerts, A., *Doctoral Dissertation*, Univ. of Antwerp, 1996.
14. Bogaerts, A. and Gijbels, R., *J. Anal. At. Spectrom.* 1997, vol. 12, p. 751.
15. Bogaerts, A. and Gijbels, R., *J. Am. Soc. Mass Spectrom.*, 1997, vol. 8, p. 1021.
16. Bogaerts, A. and Gijbels, R., *Spectrochim. Acta, Part B*, 1997, vol. 52, p. 765.
17. Bogaerts, A. and Gijbels, R., *J. Anal. At. Spectrom.*, 1996, vol. 11, p. 841.
18. Bogaerts, A., Wagner, E., and Smith, B.W., *et al.*, *Spectrochim. Acta, Part B*, 1997, vol. 52, p. 205.
19. Aston, F.W., *Proc. R. Soc. London, Ser. A*, 1907, vol. 79, p. 80.
20. van Straaten, M., Bogaerts, A., and Gijbels, R., *Spectrochim. Acta, Part B*, 1995, vol. 50, p. 583.